

Blending from binarity in microlensing searches toward the Large Magellanic Cloud

T. Blaineau¹, M. Moniez¹

Laboratoire de physique des 2 infinis Irène Joliot-Curie, CNRS Université Paris-Saclay, Bât. 100, Faculté des sciences, F-91405 Orsay Cedex, France

Received 22/03/2023, accepted 03/08/2023

ABSTRACT

Context. Studies of gravitational microlensing effects require the estimation of their detection efficiency as soon as one wants to quantify the massive compact objects along the line of sight of source targets. This is particularly important for setting limits on the contribution of massive compact objects to the Galactic halo. These estimates of detection efficiency must not only account for the blending effects of accidentally superimposed sources in crowded fields, but also for possible mixing of light from stars belonging to multiple gravitationally bound stellar systems.

Aims. Until now, only blending due to accidental alignment of stars had been studied, in particular as a result of high-resolution space images. In this paper, we address the impact of unresolved binary sources that are physically gravitationally bound and not accidentally aligned, in the case of microlensing detection efficiencies toward the Large Magellanic Cloud (LMC).

Methods. We used the Gaia catalog of nearby stars to constrain the local binarity rate, which we extrapolated to the distance of the LMC. Then we estimated an upper limit to the impact of this binarity on the detection efficiency of microlensing effects, as a function of lens mass.

Results. We find that a maximum of 6.2% of microlensing events on LMC sources due to halo lenses heavier than $30M_{\odot}$ could be affected as a result of the sources belonging to unresolved binary systems. This number is the maximum fraction of events for which the source is a binary system separated by about one angular Einstein radius or more in a configuration where light-curve distortion could affect the efficiency of some detection algorithms. For events caused by lighter lenses on LMC sources, our study shows that the chances of blending effects by binary systems is likely to be higher and should be studied in more detail to improve the accuracy of efficiency calculations.

Key words. Gravitational lensing: micro - Cosmology: dark matter - surveys - stars: binaries - Galaxy: halo - Galaxy: kinematics and dynamics

1. Introduction

Objects cataloged in dense fields are frequently composed of several blended sources. Not accounting for this may distort the statistical conclusions of the microlensing searches because of its impact on the shape of the light-curve (Stefano & Esin 1995), which can have repercussions on detection efficiency (Woźniak & Paczyński 1997). Some of the consequences of blending on microlensing have been studied by comparing ground-based images with high-resolution deep space images, obtained notably with the Hubble Space Telescope (HST) (HST archive 2002). These space images allow one to quantify the impact of accidental alignments of sources in the catalogs of the ground-based surveys, due to the high density of the field (Alibert, Y. et al. 2005; Tisserand et al. 2007; Wyrzykowski et al. 2010). However, in the direction of the Magellanic Clouds, a specific component of the blending remains poorly understood, which is a result of the mixing of light from multiple gravitational bound stars being too close together to be resolved, even by space telescopes, at a distance larger than $50 kpc$. Their existence is an additional cause of blending, distinct from the mixing caused by coincidental alignments. In this paper we study the possible consequences, currently poorly known, of the binarity of the Large Magellanic

Cloud (LMC) stars on the detectability of the gravitational microlensing effects they may experience. In particular, we study the case of the detection efficiency of microlensing effects due to high-mass ($> 30M_{\odot}$) Galactic halo objects, which have been recently searched in the LMC direction and excluded as a significant component of the hidden mass of the Galaxy (Blaineau et al. 2022). In section 2, we provide an overview of the fundamentals of the gravitational microlensing effect. In Section 3 we introduce the blending effects and their impact on the detection efficiency. We introduce the case of multiple sources and distinguish between three blending regimes. In section 4, we present our statistical analysis tools and show that we cannot extract statistical information on the LMC binary systems from HST images because of the separation limit. In section 5, we describe our methodology to estimate upper values of the binarity rate in the local volume (at a distance of less than $500 pc$). We show how the distribution of distances between the components of star pairs in a complete Gaia catalog population allows us to quantify the rate of widely separated double systems in the Galactic plane. We explain how we extrapolated the local binarity rate down to $50 au$ separations for stars closer than $500 pc$ to the Sun in section 6. In section 7, we detail how we estimated a conservative upper limit of the impact of binarity on the microlensing detection efficiency toward the LMC as a function of the projected lens Einstein radius. We discuss the validity domain and limita-

Send offprint requests to: M. Moniez,
e-mail: marc.moniez@ijclab.in2p3.fr

tions of our study, and address the question of the dependence of binarity rates on the stellar type in Section 8. We conclude and summarize our results in Section 9, and propose some prospects for future microlensing surveys.

2. Overview of microlensing

2.1. Description of a microlensing event

The gravitational microlensing effect (Paczynski 1986), which was first discovered in 1993 (Alcock et al. 1993; Aubourg et al. 1993; Udalski et al. 1993), occurs when a massive compact object (the lens) passes close enough to the line of sight of a background source and temporarily magnifies its brightness. Reviews of the microlensing formalism can be found in Schneider et al. (2006) and Rahvar (2015). When a single point lens of mass M_L located at distance D_L deflects the light from a point source located at distance D_S , a situation hereafter referred to as Point-Source Point-Lens (PSPL) event, an observer receives light from two images not separated in the telescopes. The total magnification $A(t)$ of the apparent luminosity of the source at time t is given by the following (Paczynski 1986):

$$A(t) = \frac{u(t)^2 + 2}{u(t) \sqrt{u(t)^2 + 4}}, \quad (1)$$

where $u(t)$ is the distance of the lens to the undeflected line of sight, divided by the Einstein radius r_E ,

$$r_E = \sqrt{\frac{4GM_L}{c^2} D_S x(1-x)} \simeq 4.5 \text{ au} \times \left[\frac{M_L}{M_\odot} \right]^{\frac{1}{2}} \left[\frac{D_S}{10 \text{ kpc}} \right]^{\frac{1}{2}} \frac{[x(1-x)]^{\frac{1}{2}}}{0.5}. \quad (2)$$

Here G is the Newtonian gravitational constant, and

$$x = D_L/D_S. \quad (3)$$

If the point lens has a constant relative transverse velocity v_T with respect to the point source (PSPL rectilinear event) and $u(t)$ reaches its minimum value u_0 (impact parameter) at instant t_0 , then

$$u(t) = \sqrt{u_0^2 + (t - t_0)^2/t_E^2}, \quad (4)$$

where $t_E = r_E/v_T$ is the lensing timescale,

$$t_E \sim 79 \text{ days} \times \left[\frac{v_T}{100 \text{ km/s}} \right]^{-1} \left[\frac{M_L}{M_\odot} \right]^{\frac{1}{2}} \left[\frac{D_S}{10 \text{ kpc}} \right]^{\frac{1}{2}} \frac{[x(1-x)]^{\frac{1}{2}}}{0.5}. \quad (5)$$

In the case of the study of a population of stellar sources within the LMC, and assuming that independently of their mass the lenses are distributed in a spherical, isotropic, and isothermal halo with the density distribution described in Griest (1991) and with the parameters used in Blaineau et al. (2022) (hereafter called the standard Galactic halo), the average duration of the events due to the lenses of a given mass M_L is $\langle t_E \rangle \sim 63 \text{ days} \times \sqrt{M_L/M_\odot}$.

2.2. Optical depth, event rate, and detection efficiency

The microlensing optical depth τ is defined as the probability that the line of sight to a source is within one r_E of a lens (corresponding to $A_{\max} > 1.34$ according to Eq. (1)). The event rate is the number of microlensing events per star per unit time with

$u_0 < 1$. This rate is related to the optical depth by the following relation: $\Gamma = (2/\pi)\tau/\langle t_E \rangle$ (Griest 1991). The event rate is estimated from the duration distribution of the observed events, and it must take into account the observational average detection efficiency that depends a priori on the time sampling, the photometric accuracy, the source population, the background noise, and the search algorithm. The probability of detecting a given event depends on the parameters of this event (u_0 , t_0 , t_E , and source magnitude), and the efficiency $\epsilon(t_E)$ is defined as the ratio between the following two numbers: The numerator is the sum of the detection probabilities of all events with a measured duration t_E and a measured $u_0 < 1$ (regardless of their other parameters), and the denominator is the total number of expected events with true duration t_E , true $u_0 < 1$, and true t_0 within the survey duration. This efficiency is usually calculated by a Monte-Carlo simulation of microlensing events, combined with observed light-curves of stable stars to produce realistic light-curves of microlensing events, and then subjected to the same analysis as the real data.

Basic Monte-Carlo efficiency estimates assume that the events are of the PSPL rectilinear type, that is that the magnification curve is given by equations (1) and (4). Concerning the studies toward the LMC, it has been established that the contribution of the events that could escape detection due to lens binarity does not exceed 10% (Mróz et al. 2019); the impact of the parallax effects (due to the orbital motion of the Earth around the Sun), which distort the magnification curve, is also negligible toward the LMC (Blaineau & Moniez 2020). The subject of this paper is to explore the impact of blending (see Fig. 1) on the detection efficiency toward LMC, taking into account not only the blending of accidentally aligned sources already discussed in several works (see for example Tisserand et al. (2007) and Wyrzykowski et al. (2011)), but also the – non-accidental – contribution of multiple gravitationally bound stellar systems that cannot be directly estimated from LMC spatial images.

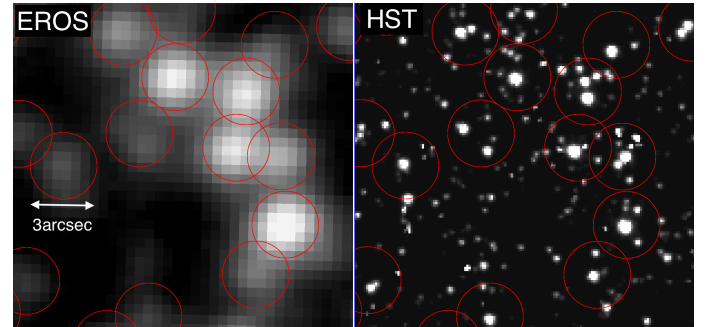


Fig. 1: Images of the same (dense) region of the LMC taken with the EROS camera (left) and the WFPC2 HST camera. The circles are centered on the EROS2 cataloged sources. It is clearly visible that several sources resolved in the HST image can merge into a single EROS cataloged object. We note that even in the HST image, the contribution of hypothetical binary systems is not resolved, and it exceeds the expectation of a random spatial distribution (see Sect. 5).

3. Blending effects in microlensing searches: The unknown contribution of binary stars

In the case where a star, whose flux ϕ_1 is amplified by a microlensing effect by a factor $A(t)$, is mixed with the light of one

or more other stars whose summed flux is ϕ_2 , the evolution of the total flux of the source is the following:

$$\phi(t) = \phi_1 A(t) + \phi_2. \quad (6)$$

By defining the blend fraction as the ratio $f_b = \frac{\phi_1}{\phi_1 + \phi_2}$,

$$\phi(t) = (f_b A(t) + (1 - f_b)(\phi_1 + \phi_2)). \quad (7)$$

If ignored – that is using the PSPL approximation –, blending may affect the efficiency of a microlensing search in several ways. On the one hand, the fact that a cataloged object is made up of light from several unresolved stars must be taken into account when estimating the effective number of stars monitored. A microlensing event can indeed occur on each of the stars composing the cataloged source, increasing the number of stars actually susceptible to lensing compared to the number of sources counted in the catalog. On the other hand, the light contribution of other stars modifies the shape of the observed light-curve from a microlensing event, in a way that changes with the passband. The efficiency of the search algorithms may then be affected by the following effects:

The shape of the light-curve can no longer be exactly fitted by that of a simple (PSPL) event, which could cause events to be missed with a low-tolerance algorithm if blending is ignored. In particular, the apparent or effective magnification A_{eff} of the object as observed from the ground is the following:

$$A_{\text{eff}}(t) = \frac{\phi(t)}{\phi_1 + \phi_2} = f_b(A(t) - 1) + 1, \quad (8)$$

then

$$\frac{A_{\text{eff}}(t) - 1}{A(t) - 1} = f_b < 1, \quad (9)$$

showing that the apparent magnification of the observed object is systematically lower than the real magnification $A(t)$ of the lensed star at all times (Stefano & Esin 1995). Therefore, the measured (or apparent) impact parameter u_0 is larger than the physical (true) impact parameter.

As soon as the blend is composed of stars of different colors, the apparent magnification is no longer achromatic: This could reduce the efficiency of a search algorithm that would only consider achromatic events.

The apparent Einstein duration t_E estimated by fitting the light-curve of a blended event with the curve of a PSPL event is systematically shorter than its real value. Since the efficiency of the analysis depends on the measured duration of the event, this means that there is also a modification of the expected number of events as a function of the duration.

All of these effects may impact the number of expected events in a nontrivial way and can potentially modify it, so it is necessary to properly take this blending effect into account for the interpretation of microlensing effect searches, especially when evaluating the optical depths. Mróz et al. (2017) have established that a complete fit of the flux light-curve – that is to say beyond PSPL approximation –, which takes a blend fraction into account as in Eq. (7), is able to reconstitute the correct parameters with no bias. However, the increase in the number of potential sources and the reduced sophistication of detection algorithms mean that detection efficiency can be affected by blending.

As previously mentioned, the confusion of several stars in a single cataloged object has several possible origins: The superposition may be due to an accidental alignment (accidental blending), depending on the field crowding, or it may be due

to the multiplicity of the stellar systems (mainly binary blending). The estimation of accidental blending, as it is classically obtained, makes the assumption of a locally uniform density distribution of stars; on the other hand, the impact of superposition due to multiple systems, the binary blending, cannot be estimated in the same way.

Considering the case of two stars blended into a single catalog object, we distinguish three blending regimes depending on their angular separation δ :

- As long as δ is large compared to both angular Einstein radii of the lens configurations¹, we can consider the two stars as independent in the context of the calculation of the expected number of events: We refer to this mixing regime as classic or ordinary since it is the one that occurs almost exclusively in the case of accidental mixing, and we then observe the addition of a constant flux to an amplified flux. Previous studies have shown that the impact of this blending regime is small ($< 10\%$) and positive on the detection efficiency (Wyrzykowski et al. (2011); Blaineau et al. (2022) and references included).
- If the angular separation δ between the two stars is small compared to the angular Einstein radii of both lens configurations, then both components undergo the same apparent magnification simultaneously, and everything happens as if a single star with a flux equal to the sum of the two stellar fluxes undergoes a PSPL microlensing effect, as in the absence of blending. According to simple geometrical considerations, this regime has a negligible probability of occurring for accidental blending, but not in the case of blending due to binarity. In the latter case, the Einstein radii are identical for the microlensing of both stars. Ignoring this blending regime has no consequence on the optical depth measurement.
- If the angular separation δ between the two stars is on the order of the angular Einstein radii of both lens configurations, then that would be an intermediate regime, where the light-curve can neither be described by a PSPL microlensing effect nor by the addition of a constant flux to an amplified flux. In this case, we observe the superposition of two events, with different magnifications, and maxima shifted in time. Depending on the geometrical configuration, two clearly separated peaks or a single asymmetric peak may appear. Several examples of magnification curves are shown in Fig. 2, with the corresponding geometrical configurations of sources and deflectors. As with the previous regime, this situation can occur only in the case of blending due to binarity, and the Einstein radii are identical for the microlensing of both stars. Only this regime is likely to cause complications when estimating the average detection efficiency of microlensing effects. If there were no physical reason for binary systems to exist, this configuration would be extremely rare and could be neglected since the probability of such a small angular distance between uncorrelated objects, even in the densest fields, is negligible. But when we are dealing with multiple gravitationally bound systems, this situation can happen more frequently.

The blending has been studied with the help of HST data, in two different ways; in the galactic plane direction, some authors (for example Rahal et al. (2009)) have used the HST images directly to associate objects detected on the ground with stars detected in HST, enabling the content of objects to be studied statistically.

¹ If the two stars are not at the same distance D_L , then the Einstein rings for microlensing by the same given lens are different.

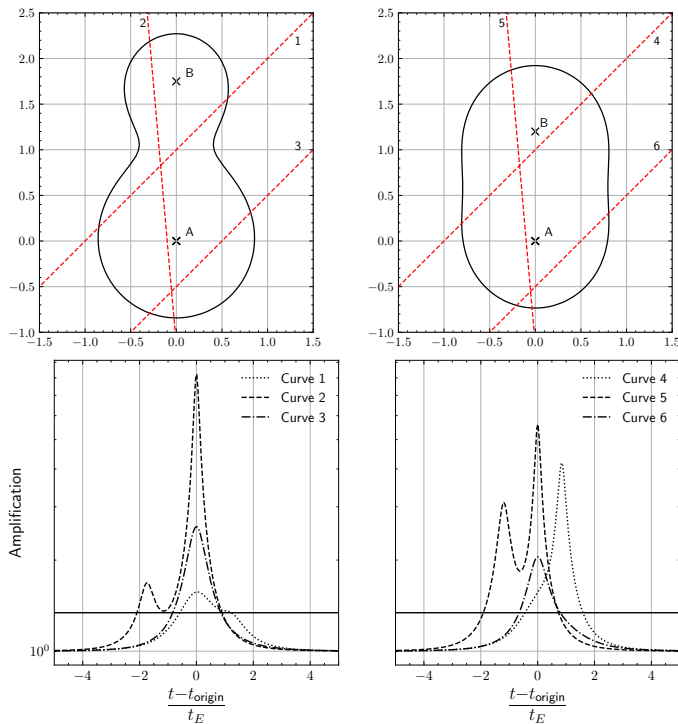


Fig. 2: Lens paths and associated light-curves.

(top) Three different trajectories of a deflector (red dashed) in front of the two stars A and B blended into a single cataloged source; on the left, stars A and B share 80% and 20% of the total luminous flux, respectively, and on the right both stars have the same luminosity. The black outline corresponds to the positions where the deflector must be for the source system to undergo a total magnification of 1.34. The coordinates are in units of Einstein radius, which is the same for both stars (located at the same distance).

(bottom) Magnification curves of the cataloged source system corresponding to the trajectories above, which travelled from left to right. The black line corresponds to a magnification of 1.34. We note that t_{origin} is the time when the deflector is closest to the star A (and thus does not always coincide with the time of maximum apparent amplification). Curves 3 and 6 are very close to microlensing curves with ordinary blending because the deflector passes far from star B.

The advantage of this approach is that it benefits from the true spatial distribution of objects, taking any nonuniformity into account, and it is limited only by the resolution of HST. The other way of using HST data is indirect, and is based on extracting the luminosity function of stars up to 3 magnitudes beyond the detection limit of ground-based surveys. Ground-based telescope images were simulated by injecting stars according to this luminosity function, and the star content of reconstructed objects was then statistically estimated. Authors using the latter technique assumed that the spatial distribution of stars is uniform and neglected the fact that the existence of bound systems results in an excess probability of small separation between components compared to a random distribution (Alibert, Y. et al. 2005; Smith et al. 2007; Tisserand et al. 2007; Wyrzykowski et al. 2010). As far as the LMC is concerned, neither approach can take the case of binary systems into account because at the LMC distance ($49.59 \pm 0.09 \pm 0.54$ kpc (Pietrzyński et al. 2019)) no excess of star

pairs can be detected with respect to a random uniform distribution of stars in the HST images, as we show in the next section. This means that even the resolution of the space telescopes is insufficient to separate two components of a binary stellar system located at ~ 50 kpc.

To quantify the impact of multiple sources on microlensing toward the LMC, we need a way to count them, based on other data than LMC spatial images. The following section shows why the limitations of these space-based observations toward the LMC have led us to study a population of the solar environment using Gaia data (Gaia Collaboration et al. 2016).

4. Angular and physical distance separation between LMC stars detected by HST

The spatial distribution of LMC stars is not expected to be uniform if it includes multiple gravitationally bound systems. This is why we work with the distribution of the number of pairs of stars as a function of their separation (angular or spatial) and the two-point angular correlation function. The correlation function is calculated with the Landy-Szalay estimator (Landy & Szalay 1993), which compares the number of pairs in the data with the number of pairs in a simulation of a uniform spatial distribution in the same spatial domain. The other way to study multiple systems is to count the number of pairs as a function of their angular separation δ . We expect this distribution to be the sum of a contribution due to fortuitous alignments and an excess at the smallest values of δ if there are multiple gravitationally bound systems in the set of the pairs. From simple geometrical considerations, the first contribution is a distribution which increases linearly with δ as long as δ is small enough so that edge effects do not limit the catalog used. The second contribution, when it exists, is expected for smaller values of δ .

Figure 3 shows the distribution of the number of pairs (top) and the two-point correlation function (bottom), as a function of the angular separation δ of the stars detected by the SExtractor algorithm (Bertin & Arnouts 1996) on an image of a crowded field of the LMC. This image has been obtained by coadding the images taken with the f555w and f814w filters by the Wide Field Planetary Camera 2 (WFPC2) of HST² (HST archive 2002). We notice that the correlation function remains zero down to the HST resolution limit (about $0.5''$), decreases below $0.5''$, and is -1 below $0.25''$, which indicates that the algorithm can never resolve two stars separated by less than $0.25''$. Since there is no positive correlation for small separations, this shows that we also do not detect an excess of pairs in the HST data over a random distribution beyond a separation of $0.5''$, which corresponds to a transverse separation of 27500 au in the LMC. This situation is not surprising since gravitationally bound systems at such distances are very rare (Dhital et al. 2010; Duchêne & Kraus 2013). The LMC is therefore too far away for HST to resolve multiple systems that would cause a significant excess of close pairs compared to a random spatial distribution.

5. Constraining the binarity rate in the LMC

Since the LMC is too far away, we studied a stellar population close to us, using data from the Gaia mission, and then we extrapolated the results to the distance of the LMC. First, we

² HST images hst_08676_08_wfpc2_f555w_wf and hst_08676_08_wfpc2_f814w_wf, at (RA, Dec) = (05h06m35.18s, $-69^{\circ}20'45.6''$).

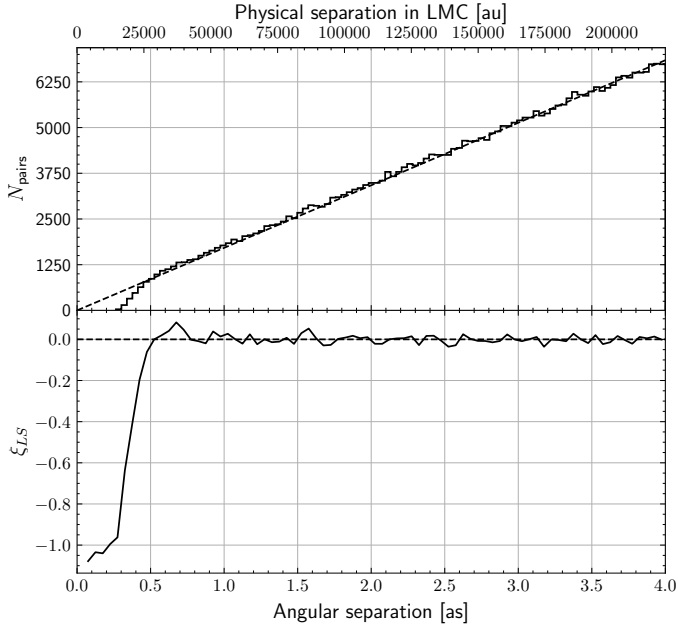


Fig. 3: Number of pairs and two-point correlation function of stars in a HST-crowded LMC field image.

(top) Number of pairs of stars per $1.2''$ interval as a function of their angular separation. The dotted line gives the predicted distribution of angular separations in the case of a spatially uniform distribution of stars with the same average star density.

(bottom) Measured two-point angular correlation function of the detected stars.

The lower scale is the angular separation δ and the upper scale gives the corresponding transverse separation in the LMC.

defined the binarity rate we used and describe our estimation method based on star pair counts.

5.1. Methodology

We wished to know the proportion of LMC objects in EROS- or MACHO-type catalogs that are binary systems as a function of their transverse separation a_t . As we have just seen, the LMC is too far away even for space missions to resolve such systems. We therefore studied a population of nearby stars cataloged by Gaia, for which the resolution of systems is possible as soon as $a_t > 500 \text{ au}$. In the following, *object* refers to an element of the Gaia catalog (which can be made of a single star or a more complex system) and *system* refers to a cluster of objects that we consider to be a gravitationally bound system (typically a resolved binary system). We then counted the binary stars in the local space, in a situation where they are well separated. We defined n_{tot}^* as the total number of objects in the catalog, and $n_{\text{bin}}^*(a_t)$ as the number of objects belonging to a resolved binary system (i.e., made of two cataloged objects), with a transverse separation $> a_t$. From these simple counts of the resolved double star systems, we could numerically compute the following function:

$$f_{\text{bin}}(a_t) = \frac{1}{n_{\text{tot}}^*} \frac{dn_{\text{bin}}^*(a_t)}{da_t}. \quad (10)$$

This function is the differential probability that a Gaia cataloged object belongs to a double system separated by a projected distance a_t . This is a function that we directly derived from the

Gaia catalog, as explained in the next sections. We then defined $F_{\text{bin}}(a_t)$, the integrated system binarity rate, as the ratio between the number of binary systems (unlike objects) with a transverse separation $> a_t$, to the total number of systems:

$$F_{\text{bin}}(a_t) = \frac{n_{\text{bin}}^*(a_t)/2}{(n_{\text{tot}}^* - n_{\text{bin}}^*) + n_{\text{bin}}^*/2} = \frac{n_{\text{bin}}^*(a_t)/n_{\text{tot}}^*}{2 - n_{\text{bin}}^*/n_{\text{tot}}^*}. \quad (11)$$

We note that the total number of systems at the denominator corresponds to the sum of the single star systems plus all the resolved binary systems – not only the systems separated by more than a_t ³. From the definition of $f_{\text{bin}}(a_t)$, we obtained

$$\frac{n_{\text{bin}}^*(a_t)}{n_{\text{tot}}^*} = \int_{a_t}^{\infty} f_{\text{bin}}(a) da, \quad (12)$$

which is the fraction of objects belonging to a binary system with a transverse separation $> a_t$. The number n_{bin}^* is the total number of objects belonging to a binary system resolved by Gaia (depending on Gaia's resolution power). This number was estimated from

$$\frac{n_{\text{bin}}^*}{n_{\text{tot}}^*} = \int_{a_t^{\text{resol}}}^{\infty} f_{\text{bin}}(a_t) da_t, \quad (13)$$

where a_t^{resol} is the separation limit of Gaia in the catalog we used. As Gaia's resolution is not a step function, we started integrating from a very small separation $a_t^{\text{resol}} = 50 \text{ au}$, below which we were sure Gaia could not separate two components, but to which we extrapolated our measurements, as shown in Section 6. This conservative choice then gave us a lower bound on n_{bin}^* , and thus an upper bound on F_{bin} in equation (11). This choice is not critical since we subsequently show that the integral (13) is much smaller than two, and it therefore has a minor impact on the denominator of Eq. (11).

5.2. Binarity of stars closer than 500 pc in the Gaia-EDR3 catalog

We have used the Gaia-EDR3 catalog (Gaia Collaboration et al. 2020) for a preliminary assessment of the impact of binarity in microlensing studies. This exploratory work does not aim to extract binarity rates, but rather upper limits on the number of multiple source systems that can give rise to complex gravitational microlensing effects. Our immediate goal is therefore to estimate the maximum fraction of binary systems separated by transverse (or projected) distances a_t comparable to or larger than the Einstein radius of a possible lens projected in the LMC.

In our definitions of the binarity rate, we have neglected the contribution of stellar systems made of more than two stars, since we find only 1% of such systems with an angular size smaller than $10''$ (corresponding to $a_t < 6000 \text{ au}$ at a 600 pc distance) in the selection of stars defined in the next paragraph. We therefore neglected this type of system in our treatment of blending effects. The estimate of the transverse (or projected) physical distance a_t of two stars in the Gaia catalog was deduced from the angular distance δ between the two components and their annual parallax measurements π , assuming that they both have an intrinsic uniform and rectilinear motion⁴ (Lindgren et al. 2012,

³ As no binary system is resolved in the LMC, we need to use this definition of a rate relative to the systems, instead of a rate relative to the – unknown – underlying number of stars.

⁴ Since we are trying to quantify binary systems, we must remember that the rotation of the stars of a system around the center of gravity

2021), by $a_t = 1 \text{ au} \times \delta/\pi$. With the parallax differences between the components being too imprecise compared to the angular accuracies, we could not carry out a study in three dimensions, which would include the longitudinal distance (along the line of sight). As we explain in the following analysis, parallaxes were just used to convert angular distances into transverse distances and also to reduce the risks of association of very distant objects, accidentally located on the same line of sight, by considering only pairs of stars with compatible parallaxes.

We selected the stars of the Gaia-EDR3 catalog (Gaia Collaboration et al. 2020), whose apparent magnitude is $3 < g < 18$, a domain in which the catalog is complete, and thus not biased (Fabricius et al. 2020). Then we limited our sample to stars closer than 600 pc (corresponding to a parallax $\pi > 1.66 \text{ mas}$). At this distance, a separation of $1''$ corresponds to 600 au . We also required that the parallax accuracy be better than 20%. The bias (Luri et al. 2018) induced by this selection can be neglected because we rejected only 2% of the stars that are the most distant of our sample. Finally, we have restricted our study to Galactic latitudes higher than 20° to avoid the very crowded and inhomogeneous areas of the Galactic plane (figure 4).

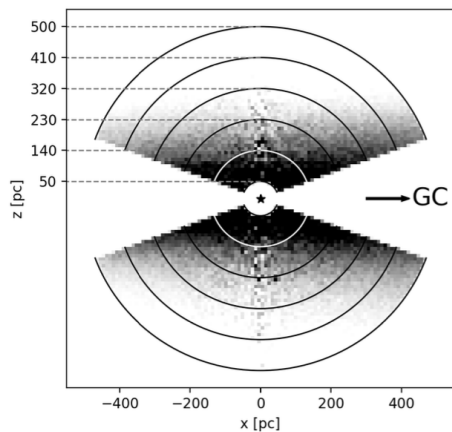


Fig. 4: Projection perpendicular to the Galactic plane of the spatial distribution of the stars of the Gaia catalog, and representation of the limits of the shells used in our study. The representation is centered on the Sun.

Figure 5 shows the distribution of the absolute magnitude G of the stars of the Gaia catalog closer than 600 pc , as a function of their distance, estimated by their parallax. This catalog is complete between the lines of equal apparent magnitude marked by the thick red curves ($g = 3$ and $g = 18$). We defined five shells (Fig. 4 and 5), delimited by the spheres of radii (50, 140, 230, 320, 410, and 500 pc), and studied the pairs of stars in each shell separately (Table 1). These five shells define a fiducial volume that is not affected by the 600 pc cutoff.

These subdivisions allowed us to verify that the separation distributions of the binaries are indeed functions of the physical distances a_t , independently of the angular distances δ , as long as they are greater than the separation power of Gaia. To ensure that the distributions studied in the five shells considered are all

alters the uniform rectilinear motion assumed in the estimation of parallaxes. As we are only interested in binary systems separated by more than 50 au , with orbital periods on the order of a few centuries, we can consider that the variation of orbital velocity on the apparent trajectory of the stars on the sky has only a negligible impact on the estimation of parallaxes in Gaia.

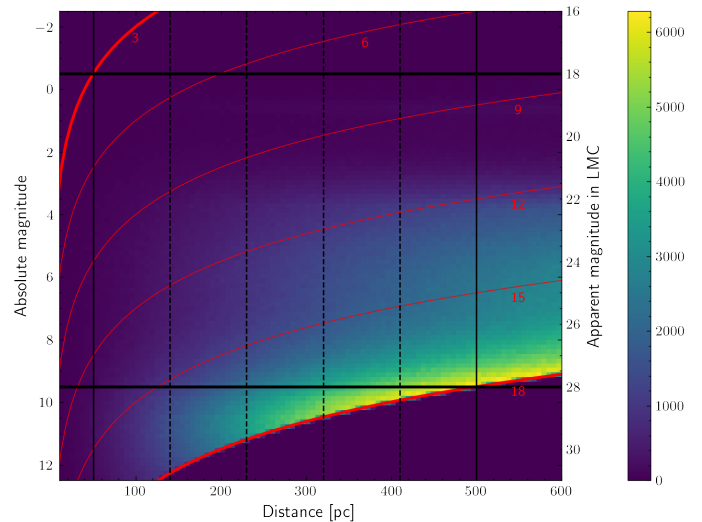


Fig. 5: Distribution of the number of stars in Gaia EDR3 as a function of their distance and absolute magnitude (left scale). The right scale gives the apparent magnitude that these stars would have in the LMC. The Gaia catalog is complete between the thick red curves. The red lines are the iso-apparent-magnitude lines in Gaia in the (distance, absolute magnitude) plane. We restricted the study to stars within the absolute magnitude range delimited by the thick horizontal black lines ($-0.5 < G < 9.5$), which ensures the homogeneity of the stellar type over the volume we considered; the vertical solid lines correspond to the distance limits of our sample. The vertical dashed black lines delineate the distance domains of the shells we consider in our analysis (between 50 and 500 pc).

shell limits	a_t for $\delta = 2''$ separation	number of stars	
		in shell	effective
[50 – 140] pc	[100 – 280] au	160409	158000
[140 – 230] pc	[280 – 460] au	481496	465000
[230 – 320] pc	[460 – 640] au	867259	807000
[320 – 410] pc	[640 – 820] au	1259719	1109000
[410 – 500] pc	[820 – 1000] au	1634717	1313000

Table 1: Limits and contents of the shells (see text).

complete, we only studied the stellar population whose absolute magnitude is in the range $-0.5 < G < 9.5$ (between the thick black lines in Figure 5). Finally, we only considered pairs of stars with a magnitude difference of less than 2.5, beyond which we could neglect the impact of the less luminous component on the light-curve of a microlensing effect.

Figure 6 shows the angular separation distribution δ for the pairs of stars closer than 600 pc . We first observed a clear excess of pairs for $\delta < 20''$, in agreement with Zavada & Pířka (2020), which demonstrates the existence of Gaia-detectable bound systems within 600 pc , in contrast to the situation in Fig. 3 which showed the inability of HST to separate bound systems in the LMC. Second, we noted that similar to HST, our algorithm failed to separate stars that are too close in angular distance, in this case around $0.5''$. The question of the separation limit, as it also relates to Gaia's scanning law, is beyond the scope of this paper (see Blaineau (2021) for more details). For our study, it is sufficient to know that we decided to focus only on pairs separated by

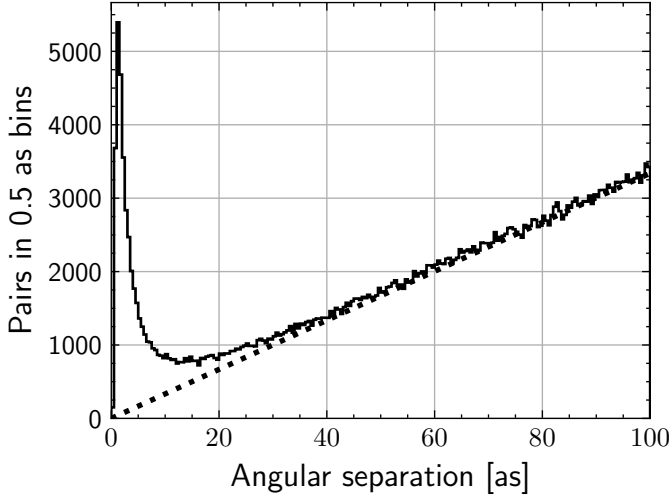


Fig. 6: Number of star pairs per $0.5''$ interval as a function of their angular separation. The dotted line gives the predicted distribution in the case of a spatially uniform distribution with the same average star density. Only stars within 600 pc of the Sun and with a Galactic latitude larger than 60° are considered here (1,233,947 stars). We measured about 29,000 pairs in excess of accidental pairs.

at least $2''$ in order not to be limited by the resolution of Gaia. We have shown that the results of the next sections vary by less than 2% (half of the estimated uncertainty) if we change this minimal separation in the range $[1.5'' - 2.5'']$ (Blaineau 2021).

To estimate the binarity rate of stars in a shell, we first built the distribution of the type shown in Figure 6. We then calculated the number of pairs remaining after subtracting the component due to accidental alignments, as a function of the separation. This expected random component is a linear function, fitted between $60''^5$ and $120''$ (dashed line in Figure 6). Once the angular separation was converted to physical transverse separation a_t (by using the measured parallax π), from the excess in each channel of a_t we could derive an estimate of the differential stellar binarity rate $f_{bin}(a_t)$ defined by expression (10), plotted in Figure 7 for each shell. We would like to remind readers that this quantity represents the differential fraction of stars in pairs in excess of the expected number of accidental pairs separated by a_t , per unit of a_t . The figure shows that the rates found do not depend on the shell considered, which allowed us to use the average distribution, weighted by the effective number of stars in each shell. These effective numbers are the numbers of stars found within the intervals of parallax of each shell, which were statistically corrected for misattributions of pairs in the shells, due to uncertainties in the measured parallaxes⁶ (see also Table 1). It should be noted that the closest shells are obviously those that allowed us to estimate the binarity rate at the smallest separations a_t , but at the expense of the statistics limited by the small volume of the shell. For shells at larger distances, the statistics is larger, but our

⁵ Two stars at $\sim 450\text{ pc}$ separated by $60''$ would be separated by only $0.5''$ if they were in the LMC. This directly illustrates the fact that an excess count of pairs in the LMC is only expected for separations much smaller than the resolution limit of HST.

⁶ These uncertainties result in uncertainties on the distance of the stars; a pair can then be either misattributed if both components are effectively in another shell, or it can be missed if only one of the components is in another shell.

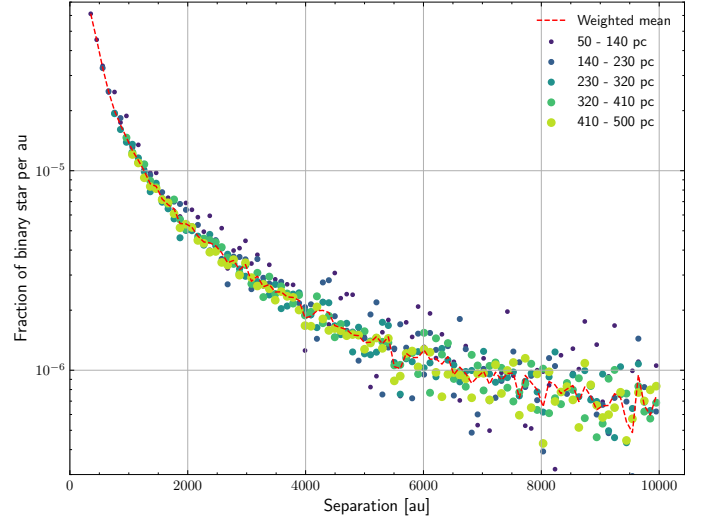


Fig. 7: Differential rate of binaries $f_{bin}(a_t)$ measured in the five shells as a function of transverse separation a_t . The red dashed line gives the means for all shells. Error bars are not shown to avoid overloading the figure, but the scatter of each series gives an indication.

angular separation limit of $2''$ prevents estimates at the smallest physical separations.

6. Estimation of the local stellar binarity rate

In this section, we explain how we fit and extrapolated the differential binarity rate down to 50 au transverse separations. Following Duquennoy & Mayor (1991) and Raghavan et al. (2010), we considered a log-normal model for the distribution of semi-major axes a of binary systems. Since we measured projected separations a_t and not semi-major axes, this distribution was modified as follows, by considering that the orbits have no preferred inclination:

$$f_{bin}^{DM}(a_t) = A \int_{a_t}^{+\infty} \frac{a_t}{r^2 \sigma \sqrt{2\pi(r^2 - a_t^2)}} \exp\left[-\frac{(\ln r/r_{mode} - \sigma^2)^2}{2\sigma^2}\right] dr, \quad (14)$$

where A and σ were fitted to our data once r_{mode} was chosen, corresponding to the maximum of the distribution. If we chose $r_{mode} = 0.1\text{ au}$, then we find $A = 0.126$ and $\sigma = 2.72$, but the fit is unsatisfactory for $a_t < 600\text{ au}$, and this is the case regardless of the parameter r_{mode} (Figure 8). This poor agreement can probably be attributed to the fact that this log-normal distribution was established for solar-type stars, while we studied a different and more extended population. Nevertheless, following this fitted model, we computed the binarity rate for systems with $a_t > 200\text{ au}$ ⁷ using Eqs (13), then (12) and (11), and found $F_{bin}(200\text{ au}) = 2.76 \pm 0.03\%$. By varying the r_{mode} parameter within $10^{-4}\text{ au} < r_{mode} < 10^2\text{ au}$, we found values close to each other, contained within $2.05\% < F_{bin}(200\text{ au}) < 2.8\%$. Similarly, we found that $F_{bin}(100\text{ au}) < 3.6\%$ regardless of the r_{mode} parameter.

⁷ This length corresponds to the most likely projected Einstein radius (at the LMC) of a $\sim 50M_\odot$ Galactic halo lens magnifying light from a LMC source.

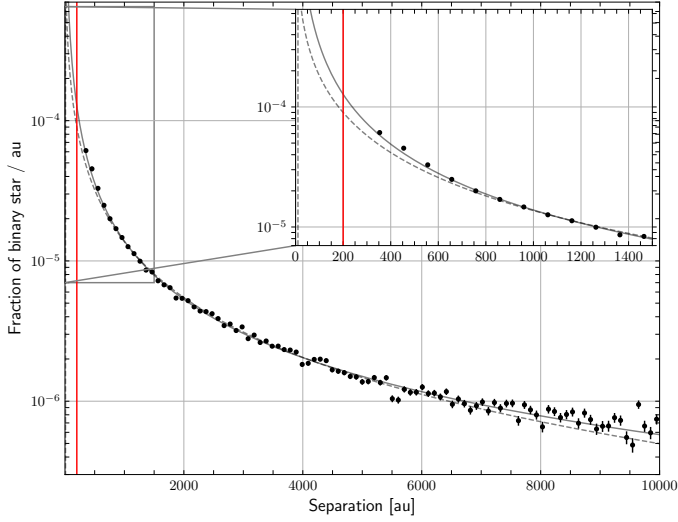


Fig. 8: Projected log-normal function f_{bin}^{DM} for $r_{mode} = 0.1 au$ (dotted line), and power function f_{bin}^{PL} (full line), fitted to the differential fraction of binary, as a function of the projected separation. The vertical red line corresponds to a projected separation of $200 au$. The inset shows that the fit of f_{bin}^{DM} is not satisfactory at small separations.

We also fitted the following empirical power-law parameterization to our measurements:

$$f_{bin}^{PL}(a_t) = (0.19 au^{-1}) \times (a_t/1 au)^{-1.379}, \quad (15)$$

which better describes our data for small a_t values (Figure 8). With this alternative model for the distribution of projected separations of binaries, we found that $F_{bin}(200 au) = 3.48 \pm 0.03\%$, a value compatible with that found with the previous model.

In section 5, we mentioned that the total probability of a Gaia object being a member of a resolved binary system is less than the value given by expression (13). The value we found by integrating Eq. (15) from $a_t = 50 au$ is 0.114, which is an upper limit of the fraction of Gaia objects belonging to binaries resolved in our sample. This number is indeed small compared to two, and its exact value does not impact the computation of F_{bin} from Eq. (11), especially since we are interested in the upper limit. It should be further noted that nothing can be said from our data about the binarity rate for $a_t < 50 au$ because extrapolation below this value is not constrained.

7. Extrapolation at the LMC; impact of binarity on microlensing detection

The previous study concerns a population of nearby Milky Way stars with $-0.5 < G < 9.5$. In the LMC, they would have an apparent magnitude $18 < g < 28$, that is they would be among the faintest stars in a classical catalog searching for gravitational microlensing effects. This is a limitation of the extrapolation of this work to observations toward the LMC, in addition to the fact that we assume that this stellar population has the same binarity statistical characteristics in the LMC as in the Milky Way disk.

We saw in section 3 that if the angular separation of the components of a blend is much smaller than the angular Einstein radius – expressed by $a_t \ll R_E/x$, where x is given by Eq. (3) –, then both sources undergo roughly the same magnification and everything happens as if there were only one source. Ignoring

this blending has therefore no impact on the detection efficiency of the ground surveys. As a consequence, only the pairs with $a_t \sim R_E/x$ or $\geq R_E/x$ should be considered for a possible impact on the statistics of microlensing effects. From the $f_{bin}^{PL}(a_t)$ function of the differential binarity rate and using Eq. (11), we can estimate the maximum proportion of situations where binarity induces a risk of failure to detect microlensing effects due to light-curve distortion. Figure 9 shows this maximum proportion

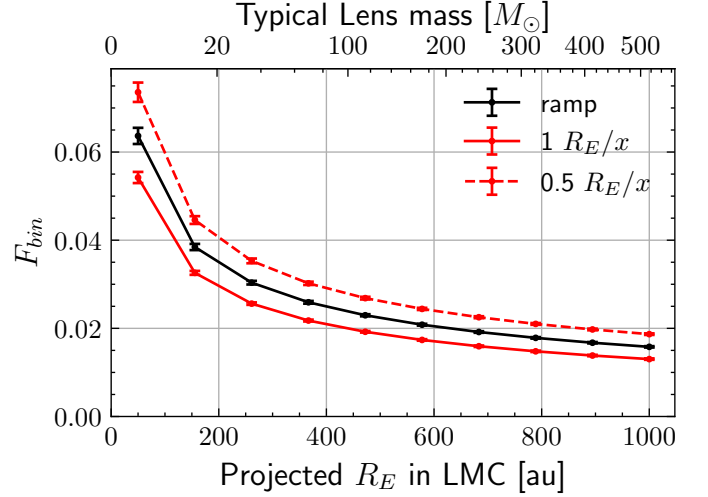


Fig. 9: Rates of binarity F_{bin} as a function of the projected Einstein radius of the lens R_E/x , obtained for different ways of integration: from a component separation larger than R_E/x (solid red line), or larger than $R_E/2x$ (dashed red line), or by weighting contributions with a ramp function (black line) (see text). Typical masses corresponding to the Einstein radii are plotted on the upper abscissa for sources within the LMC. This rate is an upper limit to the risk of not detecting microlensing effects due to binarity-induced distortion of the light-curve.

as a function of the Einstein radius projected in the LMC, R_E/x , after integration over the distribution of a_t under three different assumptions: assuming that the blend effect is significant as soon as $a_t > R_E/2x$ (and thus integrating the differential distribution from $R_E/2x$ to infinity), or only when $a_t > R_E/x$, or weighting the differential distribution between zero and one (ramping) when a_t varies from $0.1R_E/x$ to $1.75R_E/x$. The latter assumption was derived from the study of Griest & Hu (1992), which discusses the distortions expected by a microlensing curve for a composite source in detail. Figure 9 shows, for example, that under the most pessimistic assumption (a blending effect taken into account as soon as $a_t > R_E/2x$), no more than 7% of the sources are binary systems with a luminosity difference of less than 2.5 magnitude between the components, a configuration that could affect the identification of light-curves of microlensing events when $R_E/x > 50 au$.

8. Discussion

8.1. Field of application

One must first remember the limitations of this work. Only the population of stars of absolute magnitude $-0.5 < g < 9.5$ could be thoroughly studied, and any use for another population is an extrapolation, either for an identical population though in an

$M_L (M_\odot)$	1	3	10	30	100
$R_E/x < 50 \text{ au}$	71%	34%	9%	2%	0.4%
max. contribution	71%	34%	9%	2%	0.4%
$50 < R_E/x < 1000$	29%	66%	91%	97%	95%
max. contribution	1.8%	3.9%	4.6%	4.0%	4.8%
$R_E/x > 1000 \text{ au}$	0%	0%	0.2%	0.8%	5%
max. contribution	0%	0%	0%	0%	0.1%
Total	73%	38%	14%	6.2%	5.3%

Table 2: Fractions of events toward the LMC within the three domains of the projected Einstein radius and their *maximum* contributions to the fraction of events with significant blending due to binarity.

other galaxy possibly with a different metallicity, or for a stellar population in the Milky Way with more extensive types.

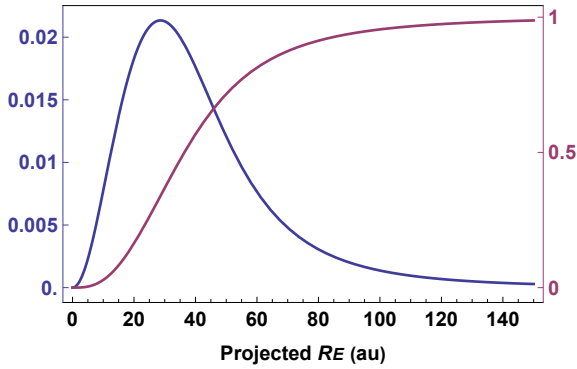


Fig. 10: Distribution of the projected Einstein radius $R_E/x = R_E D_S/D_L$ for the microlensing events toward the LMC due to $1M_\odot$ lenses within the standard Galactic halo (blue line). The distribution expected for other lens masses M_L can be obtained by scaling the abscissa by the factor $\sqrt{M_L/M_\odot}$. The purple line shows the cumulative distribution. The most probable value of R_E/x is 28.6 au, the mean is 44.0 au, and the median is 36.5 au.

To compute the fraction of potentially complex events due to binarity as a function of the lens mass, we combined the rates from Fig. 9 with the projected Einstein radius R_E/x distribution expected for that lens mass. Figure 10 shows this generic distribution for lenses of $1M_\odot$ mass, changing with M_L by simply scaling the abscissa with $\sqrt{M_L/M_\odot}$. This has been established by assuming that the lenses are spatially distributed according to the standard Galactic halo described in Blaineau et al. (2022). Table 2 shows, for a series of lens masses, the maximum expected fractions of situations where the shape of the microlensing events can be affected by binarity, splitted into three domains of projected Einstein radius R_E/x . For each lens mass, the event fraction for each domain was deduced from the properly scaled distribution of Fig. 10: For $R_E/x < 50 \text{ au}$, we conservatively assumed that 100% of the events can be affected by blending due to binarity; for $50 \text{ au} < R_E/x < 1000 \text{ au}$, we integrated the most pessimistic function of Fig. 9, weighted by the normalized distribution of R_E/x ; for $R_E/x > 1000 \text{ au}$, we considered that no more than 2% of the events can be affected by blending due to binarity.

The totals given in the table are the maximum proportions of events whose shape can be affected by binarity. This does not

necessarily mean that such events systematically escape detection (a lot depends on the selection algorithm). Nevertheless, for the sake of caution, we will keep these proportions as an upper limit for situations where the classic detection efficiency calculation does not apply. In the absence of a specific simulation, the status of these events on binaries in terms of the detection efficiency is indeed poorly known, and this must be taken into account as a systematic uncertainty for the measurement of optical depths and event rates.

Our study shows that the impact of source binarity can be neglected to first order when searching for gravitational microlensing effects from lenses heavier than $30M_\odot$. The maximum value of uncertainty of 6.2% is even smaller when the lenses are more massive (Fig. 10), showing that the additional effect of binarity on the blending effects can be neglected for heavy lenses, as was done in Blaineau et al. (2022). Figures 9 and 10 allows for these numbers to be estimated in the case of even more massive lenses toward the LMC. For an estimate corresponding to another Galactic halo model, or to other targets than LMC, Fig. 10 needs to be rebuilt.

For events due to lighter lenses with a higher probability of projected Einstein radii $R_E/x < 50 \text{ au}$, it is currently not possible to draw reliable conclusions on the impact of the blend due to the binarity of the LMC sources with our technique without risky extrapolation. An alternative method for estimating the differential binarity rate with a projected separation of less than 50 au is needed, coupled with a specific simulation to estimate the detection efficiency of non-PSPL events.

Skowron et al. (2009) found that 0.5% of the events observed by OGLE toward the Galactic Center (not LMC) have two peaks because they are due to binary systems (lens or source). This suggests that a larger proportion must suffer lesser distortions (Di Stefano & Mao 1996), but this leads in particular to them being assigned an incorrect duration, and this may affect the efficiency calculation. It is not easy to extrapolate these observations to the LMC (but see Griest & Hu (1992)), but nonetheless it seems to us that the question is not strictly closed for microlensing toward the LMC caused by light halo objects, even if it is likely that the effect we are talking about is negligible.

8.2. Discussion on stellar populations

Since the majority of the stars observed in the LMC correspond to the brightest stars in the Gaia data that we used (Fig. 5), we investigated the variation of the binarity rate $F_{bin}(200 \text{ au})$ with the magnitude of the stars. We therefore reproduced our analysis by restricting our sample to two absolute magnitude g domains, between -0.5 and 4.5 mag (3,090,000 stars) and between 4.5 and 9.5 mag (612,000 stars), always limiting the maximum difference in magnitude between the two components to 2.5. The statistical power here was significantly reduced for the population with $-0.5 < g < 4.5$, but we nevertheless found a significantly lower binarity rate for bright star pairs ($F_{bin}(200 \text{ au}) = 1.42 \pm 0.08\%$) than for faint star pairs ($F_{bin}(200 \text{ au}) = 2.58 \pm 0.04\%$). It is therefore likely that in LMC catalogs such as the EROS2 or MACHO surveys, which are composed of rather bright stars, we overestimated the binarity rate by assuming that the stellar populations from our Gaia sample and in the LMC are similar.

We also investigated whether there are correlations between the magnitude differences and the separation a_t of binaries. Figure 11 shows in green the distributions of magnitude differences ΔG between components for binaries with $1000 \text{ au} < a_t < 2500 \text{ au}$ (Fig. 11(b)) and with $a_t < 1000 \text{ au}$ (Fig. 11(c)), ob-

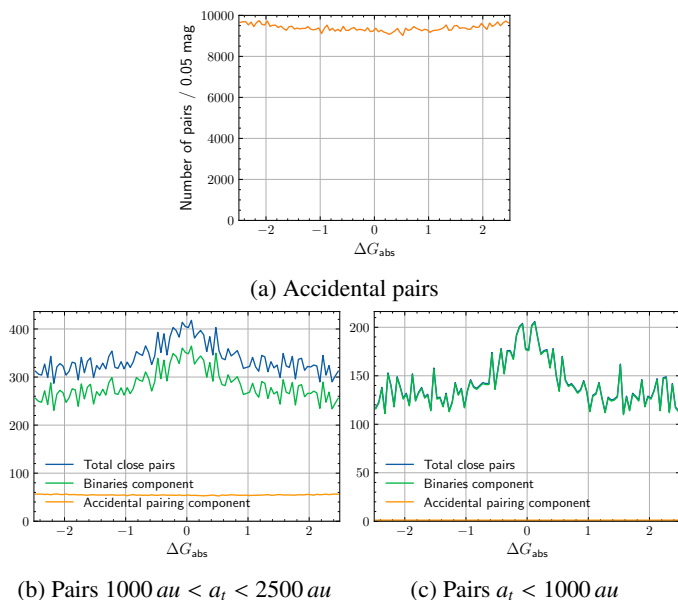


Fig. 11: Magnitude differences between components of pairs, for different separation ranges. (a) Magnitude differences for pairs separated by more than 30000 au (only due to fortuitous alignments). (b) and (c) Same distributions for pairs separated by $1000 < a_t < 2500 au$ and $a_t < 1000 au$ (blue), distributions for the fortuitous alignments (orange), normalized according to the sample size, and the difference between the two distributions (green; i.e., the distribution of the magnitude difference for binary systems only). These histograms are sampled in 0.05 magnitude steps with one entry per star. In panel (c) the number of fortuitous alignments is negligible, and thus the orange distribution is almost zero and green and blue distributions are superimposed.

tained by subtracting the expected distributions for random pairs (Fig. 11(a)), properly normalized, from the observed (blue) distributions. The distribution for random pairs was deduced from that of the difference ΔG of pairs of uncorrelated stars, separated by $a_t > 30000 au$ – which turns out to be approximately uniform. It appears that the closer the binary system is, the smaller the difference in magnitude between components. It is tempting to explain this difference by the intervention of a gravitational capture mechanism, which would favor the formation of distant binaries, whose luminosity would be consequently less correlated. These observations are corroborated by the distribution of mass ratios as a function of the semi-major axis or period of the binary systems in Moe & Di Stefano (2017).

Finally, we examined the case of red giants, which constitute an important part of the catalogs of the historical microlensing surveys to the LMC. Unfortunately, they represent too few stars in our Gaia sample to establish a reliable binarity rate. However, we examined the magnitude distribution of stars in pairs with separation $a_t < 2500 au$ containing at least one giant. In this sample of pairs, we found that there are almost no giant binary systems (less than 1% of the sample), but only binaries consisting of a giant and a main sequence star, with magnitude difference ΔG larger than 2.5 in 85% of the cases. This fact reinforces our conclusion that we probably overestimated the proportion of binaries in EROS2/MACHO-type catalogs by extrapolating the binarity rate measured in Section 7.

9. Conclusions: The impact of binarity on microlensing surveys

We conclude from this study that the search detection efficiency of long duration microlensing events due to lenses heavier than $30M_{\odot}$ toward the LMC is not significantly affected by the source binarity. This result is useful not only in the recent combined analysis of EROS and MACHO data spanning several decades (Blaineau et al. 2022), but also in future research with Rubin-LSST.

On the other hand, for lenses lighter than $30M_{\odot}$, as soon as the projected Einstein radius is less than a few tens of au , the binarity rates extrapolated here are higher and less reliable. The fraction of events that may be affected by blending due to source binarity becomes less negligible, and another study must be undertaken to estimate the impact of a binarity rate that may be more significant and probably positive on the detection efficiency.

Although it is not possible to estimate from the Gaia database the differential binarity rate for $a_t < 50 au$ in the LMC, one can conversely consider detecting binarity effects by measuring distortions due to blending with respect to a simple (PSPL) microlensing effect. The fraction of cases where a fit with blend (according to Eq. (7)) is significantly better than the PSPL fit would allow us to extract constraints on the binarity rate. This should be particularly relevant to Rubin-LSST observations if the photometric accuracy reaches a few milli-magnitudes.

Our study of the impact of binarity rates on microlensing detection efficiency toward the LMC is easily transferable, through some scaling and modelization of the lens spatial distribution, to studies of microlensing within the Galactic plane. In this case, the source population should better resemble the one studied in this paper. Our last comment is that the use of a tolerant pre-filtering, not too sensitive to the precise shape of the magnification curve, remains the safest technique to mitigate the possible effects of distortion due to the binarity of the source on the detection efficiency.

Acknowledgements. We thank Olivier Perdureau for his useful comments on the manuscript. This work was supported by the Paris Île-de-France Region.

References

- Alcock, C., Akerlof, C., Allsman, R., et al. 1993, *Nature*, 365
- Alibert, Y., Chabrier, G., & Massacrier, G. 2005, *A&A*, 442, 501
- Aubourg, E., Bareyre, P., Bréhin, S., et al. 1993, *Nature*, 365, 623
- Bertin, E. & Arnouts, S. 1996, *A&AS*, 117, 393
- Blaineau, T. 2021, PhD thesis, Ecole doctorale n°576, Particules Hadrons Energie et Noyau: Instrumentation, Image, Cosmes et Simulation
- Blaineau, T. & Moniez, M. 2020, *A&A*, 636, L9
- Blaineau, T., Moniez, M., Afonso, C., et al. 2022, *A&A*, 664, A106
- Dhital, S., West, A. A., Stassun, K. G., & Bochanski, J. J. 2010, *The Astronomical Journal*, 139, 2566
- Di Stefano, R. & Mao, S. 1996, *ApJ*, 457, 93
- Duchêne, G. & Kraus, A. 2013, *Annual Review of Astronomy and Astrophysics*, 51, 269
- Duquenois, A. & Mayor, M. 1991, *A&A*, 500, 337
- Fabriceus, C., Luri, X., Arenou, F., et al. 2020, arXiv e-prints, arXiv:2012.06242
- Gaia Collaboration, Brown, A. G. A., Vallenari, A., et al. 2020, arXiv e-prints, arXiv:2012.01533
- Gaia Collaboration, Prusti, T., de Bruijne, J. H. J., et al. 2016, *A&A*, 595, A1
- Griest, K. 1991, *ApJ*, 366, 412
- Griest, K. & Hu, W. 1992, *ApJ*, 397, 362
- HST archive. 2002, <https://archive.stsci.edu/>
- Landy, S. D. & Szalay, A. S. 1993, *ApJ*, 412, 64
- Lindgren, L., Klioner, S. A., Hernández, J., et al. 2021, *A&A*, 649, A2
- Lindgren, L., Lammers, U., Hobbs, D., et al. 2012, *A&A*, 538, A78
- Luri, X., Brown, A. G. A., Sarro, L. M., et al. 2018, *A&A*, 616, A9
- Moe, M. & Di Stefano, R. 2017, *ApJS*, 230, 15

- Mróz, P., Udalski, A., Skowron, J., et al. 2017, *Nature*, 548, 183
- Mróz, P., Udalski, A., Skowron, J., et al. 2019, *ApJS*, 244, 29
- Paczynski, B. 1986, *ApJ*, 304, 1
- Pietrzyński, G., Graczyk, D., Gallenne, A., et al. 2019, *Nature*, 567, 200
- Raghavan, D., McAlister, H. A., Henry, T. J., et al. 2010, *ApJS*, 190, 1
- Rahal, Y. R., Afonso, C., Albert, J. N., et al. 2009, *A&A*, 500, 1027
- Rahvar, S. 2015, *International Journal of Modern Physics D*, 24, 1530020
- Schneider, P., Kochanek, C., & Wambsganss, J. 2006, *Gravitational Lensing: Strong, Weak and Micro* (Springer Berlin, Heidelberg)
- Skowron, J., Wyrzykowski, L., Mao, S., & Jaroszyński, M. 2009, *Monthly Notices of the Royal Astronomical Society*, 393, 999
- Smith, M. C., Woźniak, P., Mao, S., & Sumi, T. 2007, *Monthly Notices of the Royal Astronomical Society*, 380, 805
- Stefano, R. D. & Esin, A. A. 1995, *The Astrophysical Journal*, 448, L1
- Tisserand, P., Le Guillou, L., Afonso, C., et al. 2007, *A&A*, 469, 387
- Udalski, A., Szymanski, M., Kaluzny, J., et al. 1993, *Acta Astron.*, 43, 289
- Woźniak, P. & Paczyński, B. 1997, *ApJ*, 487, 55
- Wyrzykowski, L., Kozłowski, S., Skowron, J., et al. 2010, *Monthly Notices of the Royal Astronomical Society*, 413, 493
- Wyrzykowski, L., Skowron, J., Kozłowski, S., et al. 2011, *MNRAS*, 416, 2949
- Zavada, P. & Přška, K. 2020, *AJ*, 159, 33